Check for updates

AGU ADVANCING EARTH AND SPACE SCIENCES

Geophysical Research Letters

RESEARCH LETTER
10.1029/2023GL106540

Reducing Resolution Dependency of Dust Emission Modeling Using Albedo-Based Wind Friction

Adrian Chappell[1], Mark Hennen[2], Kerstin Schepanski[3], Saroj Dhital[4], and Daniel Tong[5]

[1]School of Earth and Environmental Science, Cardiff University, Cardiff, UK, [2]Catapult Satellite Services, Oxford, UK, [3]Institute of Meteorology, Freie Universität Berlin, Berlin, Germany, [4]USDA-ARS Jornada Experimental Range, Las Cruces, NM, USA, [5]Department of Atmospheric, Oceanic and Earth Sciences, George Mason University, Fairfax, VA, USA

Abstract Numerical simulations of dust emission processes are essential for dust cycle modeling and dust-atmosphere interactions. Models have coarse spatial resolutions which, without tackling sub-grid scale heterogeneity, bias finely resolved dust emission. Soil surface wind friction velocity (u_{s*}) drives dust emission non-linearly with increasing model resolution, due mainly to thresholds of sediment entrainment. Albedo is area-integrated, scales linearly with resolution, is related to u_{s*} and hence represents its sub-grid scale heterogeneity. Calibrated albedo-based global dust emission estimates decreased by only 2 Tg y^{-1} (10.5%) upscaled from 0.5 to 111 km, largely independent of resolution. Without adjusting wind fields, this scaling uncertainty is within recent estimates of global dust emission model uncertainty (±14.9 Tg y^{-1}). This intrinsic scaling capability of the albedo-based approach offers considerable potential to reduce resolution dependency of dust cycle modeling and improve the representation of local dust emission in Earth system models and operational air quality forecasting.

Plain Language Summary Global computer models for atmospheric dust were developed to understand the global dust cycle. However, these coarse resolution global dust models cannot accurately represent small-scale dust emission processes and partly cause different dust emission estimations between the models. Using our new approach based on satellite products, we show that global dust emission estimation is largely independent of model resolution.

Key Points:

- Wind friction velocity calibrated to linearly upscaled albedo was largely independent of model resolution between 0.5 and 111 km
- Without modifying wind fields, global dust emissions decreased by only 10.5% (within model uncertainty) from 0.5 to 111 km model resolution
- Sub-grid scale heterogeneity is necessary to accurately represent grain-scale sediment supply and entrainment in large scale modeling

Supporting Information:

Supporting Information may be found in the online version of this article.

Correspondence to:

A. Chappell,
chappella2@cardiff.ac.uk

Citation:

Chappell, A., Hennen, M., Schepanski, K., Dhital, S., & Tong, D. (2024). Reducing resolution dependency of dust emission modeling using albedo-based wind friction. *Geophysical Research Letters*, *51*, e2023GL106540. https://doi.org/10.1029/2023GL106540

Received 24 JULY 2023
Accepted 11 FEB 2024
Corrected 20 MAR 2024

This article was corrected on 20 MAR 2024. See the end of the full text for details.

Author Contributions:

Conceptualization: Adrian Chappell, Mark Hennen
Formal analysis: Adrian Chappell
Investigation: Adrian Chappell
Methodology: Adrian Chappell, Mark Hennen, Kerstin Schepanski
Software: Adrian Chappell
Visualization: Mark Hennen
Writing – original draft: Adrian Chappell, Kerstin Schepanski
Writing – review & editing: Adrian Chappell, Mark Hennen, Saroj Dhital, Daniel Tong

© 2024. The Authors.
This is an open access article under the terms of the Creative Commons Attribution License, which permits use, distribution and reproduction in any medium, provided the original work is properly cited.

1. Introduction

Atmospheric mineral dust impacts Earth's systems, human health, and global economies (Tegen and Schepanski, 2018; Li et al., 2018; Pi et al., 2020). Global dust models were developed more than two decades ago (Joussaume, 1990; Marticorena and Bergametti, 1995; Shao et al., 1996) to resolve spatial patterns and trends of aeolian processes in the dust cycle (Shao et al., 2011). These models are essential for palaeo-environmental reconstructions (Mahowald et al., 2010), dust-climate interactions (Albani et al., 2014; Shao et al., 2013) air quality applications, and dust-atmosphere interactions (Wilcox et al., 2010). These global dust cycle models have coarse horizontal resolutions. Applying a single mean wind speed to these large pixels can bias dust emission (F) model simulations depending on the sub-grid scale heterogeneity of the wind friction velocity (Raupach and Lu, 2004; Ridley et al., 2013). The inability of the coarse resolution to resolve the fine resolution processes, challenges the accurate estimation of F trends and patterns (Meng et al., 2021). Dust emission is dependent on horizontal sediment flux (Q) and the sandblasting process which is influenced by the entrainment threshold (u_{*ts}). The magnitude and frequency of processes that cause u_{*ts} to be exceeded depend on the soil surface wind friction velocity (u_{s*}) transferred from above the largest roughness scale, typically controlled by vegetation. The physics of wind-blown F (Shao et al., 2011) are typically at the grain-scale (Raupach and Lu, 2004). These are point "support", following the geostatistical literature, where "support" is the volume of measurement (Kyriakidis and Yoo, 2005). For clarity, the u_{*ts} is point support which should be compared with the point support u_{s*} for compatibility, to calculate Q and F. Regional and global F models are driven by coarse resolution wind fields modeled over an area or pixel support. Despite being provided on a regular grid, these wind fields are not point support and are therefore incompatible with grain-scale physics and parameterizations (Gotway and Young, 2002) used in Q and F models (Leung et al., 2023; Meng et al., 2021; Raupach and Lu, 2004; Ridley et al., 2013). For clarity, we use model resolution to refer to different sized areal data or pixel support and in our work we do not use the terms "grid resolution" and "grid spacing" to avoid giving the impression that these data

19448007, 2024, 5, Downloaded from https://agupubs.onlinelibrary.wiley.com/doi/10.1029/2023GL106540 by Freie Universitaet Berlin, Wiley Online Library on [12/04/2024]. See the Terms and Conditions (https://onlinelibrary.wiley.com/terms-and-conditions) on Wiley Online Library for rules of use; OA articles are governed by the applicable Creative Commons License

are point support. To address the problem of missing F due to the smoothing of the sub-grid wind maxima, a common approach is to employ a gridded Weibull distribution (Cakmur et al., 2004; Cowie et al., 2015; Grini et al., 2005; Menut, 2018; Tai et al., 2021; Zhang et al., 2016). Meng et al. (2021) developed and applied a method to harmonize F across simulations of different resolutions by generating offline F from fine resolution meteorological fields. Leung et al. (2023) proposed an alternative approach to derive a simple spatial map and upscale the spatial variability of F from fine to coarse resolution.

Aerodynamic roughness depends on wind speed and responds to roughness element height, width and configuration. As area increases, roughness elements are not linearly additive because of their mutual sheltering caused by their configuration. Consequently, aerodynamic roughness does not scale linearly with increasing area. Raupach and Lu (2004) showed incisively that the scaling problem of F models can be resolved by parameterizing hard-to-measure variables for example, wind friction velocity, with more widely available, area-integrated data for example, albedo which scales linearly with increasing area. This approach was implemented recently for the calculation of the areal soil surface wind friction velocity (u_{s*}) using a calibration with albedo which scales linearly over increasing area (Chappell and Webb, 2016; Ziegler et al., 2020; Zhou et al., 2024). The calibration is applied after the albedo is scaled to the desired resolution to overcome the non-linearity of upscaling u_{s*}. This albedo-based approach was developed for use across scales from ground-based to Earth System Models (ESMs), wherever albedo data are available. It enables correctly upscaled, area-weighted estimates of u_{s*} for calculating Q and F demonstrated using MODIS albedo daily, every 500 m across Earth (Chappell and Webb, 2016; Chappell et al., 2019; Hennen et al., 2022). This albedo-based approach improves regional dust model performance with better representation of roughness (LeGrand et al., 2023). This approach offers the opportunity to investigate the extent to which existing regional and global Q and F models are resolution dependent, constrained by the incompatibility of the grain-scale model and the areal wind fields.

This scaling issue at least partially explains why there are several orders of magnitude difference in updated global F estimates (29–4,313 Tg y^{-1} up to 20 μm particle diameter (Chappell, Webb, Hennen, Schepanski, et al., 2023; Huneeus et al., 2011)). Ridley et al. (2013) suggested that the fidelity of F modeling may benefit from better representation of these roughness and texture properties and consideration of their sub-grid distribution. The arising hypothesis is therefore that compatibility between areal wind fields and areal u_{s*} should improve the performance of F modeling across scales (Chappell, Webb, Hennen, Schepanski, et al., 2023).

2. Materials and Methods

2.1. Theoretical Basis for Scaling Using Linearly Additive Surrogate Space-Time Data

Large uncertainty occurs in coarsely resolved modeling due to sub-grid scale heterogeneity (de Vrese and Hagemann, 2016). That heterogeneity is always much larger than any coarsely resolved model (Raupach and Lu, 2004). Consequently, processes occurring at fine resolution are typically described by relations and variables applicable at single points. Raupach and Lu (2004) denote these grain-scale models by $f = f(\boldsymbol{v})$, where f is a flux for example, F, and $\boldsymbol{v}$ a vector of driving variables determining the flux for example, u_{s*}. However, models require parameterizations between fluxes and variables averaged spatially over model unit areas (pixels) and temporally over model time steps that is, $\overline{f} = \overline{f}(\overline{\boldsymbol{v}})$, where overbars denote space-time averaging. The scaling problem of how to obtain $\overline{f}(\overline{\boldsymbol{v}})$ from $f(\boldsymbol{v})$, is not solved by simply averaging, resampling or interpolating from one grid spacing to another (Leung et al., 2023; Ridley et al., 2013). Scaling requires the conversion of point support to area support (de Vrese and Hagemann, 2016; Kyriakidis and Yoo, 2005; Raupach and Finnigan, 1995; Van Looy et al., 2017). Raupach and Lu (2004) succinctly describe the scaling problem as finding

$$\overline{f} = \int f(\boldsymbol{v})\, p(\boldsymbol{v})\, d\boldsymbol{v}, \tag{1}$$

where $p(\boldsymbol{v})$ is the probability density function of $\boldsymbol{v}$ in a pixel. Following Raupach and Lu (2004), there are two cases of the scaling problem. The first case is relatively trivial where the grain-scale model $f(\boldsymbol{v})$ is a linearly additive form of fluxes and driving variables. The second more challenging case is when the grain-scale model $f(\boldsymbol{v})$ is non-linear, common in aeolian transport modeling. In this latter non-linear case, either the grain-scale model $f(\boldsymbol{v})$ and averaged models $\overline{f}(\overline{\boldsymbol{v}})$ have different functional forms, or the averaged quantities $\left(\overline{f}, \overline{\boldsymbol{v}}\right)$ are not related to the grain-scale by linear averages. The origin of the problem is the combined influence of non-linearity in $f(\boldsymbol{v})$ and

19448007, 2024, 5, Downloaded from https://agupubs.onlinelibrary.wiley.com/doi/10.1029/2023GL106540 by Freie Universitaet Berlin, Wiley Online Library on [12/04/2024]. See the Terms and Conditions (https://onlinelibrary.wiley.com/terms-and-conditions) on Wiley Online Library for rules of use; OA articles are governed by the applicable Creative Commons License

statistical variability in $\boldsymbol{v}$ (Equation 1). This causes the scaling problem to be dependent on the sub-grid scale heterogeneity through the $p(\boldsymbol{v})$ of the driving variables $\boldsymbol{v}$.

Raupach and Lu (2004) described the most effective way to acquire sufficient spatially distributed information of sub-grid scale heterogeneity in $p(\boldsymbol{v})$. Their recommendation was to constrain spatial patterns in parameters by using readily available data which is spatially correlated with hard-to-measure properties for example, u_{s*}. Consistent with Equation 1, this approach amounts to estimating $p(\boldsymbol{v})$ by using surrogates, for which space-time information is available to determine spatial patterns in $\boldsymbol{v}$. We follow this approach using the albedo-based relation with u_{s*} for scaling F modeling.

2.2. Dust Emission Modeling Using Areal Albedo-Based u_{s*}

The flux $f(\boldsymbol{v})$ of point support dust emission F (kg m^{-2} s^{-1}) is reliant on grain-scale sediment flux Q (kg m^{-1} s^{-1} (Namikas and Sherman, 1997)) and calculated using the albedo-based approach (AEM)

$$Q_{AEM}(d,w,\omega,U_h)=\begin{cases} c\dfrac{\rho_a}{g}u_{s*}^3(\omega,U_h)\left(1+\dfrac{u_{*ts}(d)H(w)}{u_{s*}(\omega,U_h)}\right)\left(1-\left(\dfrac{u_{*ts}(d)H(w)}{u_{s*}(\omega,U_h)}\right)^2\right), u_{s*}>u_{*ts}H(w). \\ 0, u_{s*}\le u_{*ts}H(w) \end{cases} \quad (2)$$

That flux has driving variables ($\boldsymbol{v}$; Equation 1) over typically large (e.g., >11 km) areas with sub-grid scale heterogeneity in u_{s*}, with the momentum remaining at the soil surface after removing the influence of roughness at all larger scales. The areal coupled parameter u_{s*}/U_h is retrieved at any scale by using the linear scaling relation with albedo (ω; Equation S1 in Supporting Information S1) with an estimation uncertainty of 0.0027 m s^{-1} (Chappell & Webb, 2016; Text S1 in Supporting Information S1). The Q_{AEM} requires u_{s*} enabled by multiplying u_{s*}/U_h with near surface areal mean wind speed (U) for a given height h (where U_h is typically resolution dependent). The $u_{*_{ts}}(d)$ is a grain-scale entrainment threshold wind friction velocity (m s^{-1}). The $u_{*_{ts}}$ (Marticorena and Bergametti, 1995) and its adjustment using $H(w)$, a function of soil moisture (w) which inhibits entrainment (Fécan et al., 1999), are both described in standard workflows (Darmenova et al., 2009) and in Text S2 in Supporting Information S1. For simplicity, ρ_a air density (1.23 kg m^{-3}), g gravitational acceleration (9.81 m s^{-2}), and $c = 1$ is a dimensionless fitting parameter. The classical Q_{TEM} uses u_* described in standard workflows (Darmenova et al., 2009) and in Supplement S2. The classical Q_{TEM} approach requires the drag partition $R(z_0,z_{0s}) = u_{s*}/u_*$ which is poorly constrained with aerodynamic roughness lengths (z_0,z_{0s}) typically (Zender et al., 2003) fixed over space and static over time ($z_0 = 100$ μm and $z_{0s} = 33.3$ μm), which fixes $R \approx 0.91$ and the magnitude of Q_{TEM} is also over-estimated by using u_* cubed (Chappell, Webb, Hennen, Zender, et al., 2023; Webb et al., 2020).

2.3. Dust Emission Modeling

The albedo-based dust emission flux (F_{AEM} for particles <10 μm; kg m^{-2} s^{-1}) is calculated as a function of soil clay content (Marticorena and Bergametti, 1995)

$$F_{AEM}(\omega)=\sum_d A_f A_s M Q_{AEM} 10^{(0.134\ \%_{clay}-6.0)} \text{ with } 0\%<\text{clay}\%<20\%. \quad (3)$$

We restricted clay% to a maximum value of 20% consistent with previous work (Marticorena and Bergametti, 1995). The Q_{AEM} producing dust, is adjusted by the emitted dust fraction M for a given particle size fraction with diameter d which we calculated as $0.1 < d < 10$ μm (Zender et al., 2003) by using $M = 0.87$. The F of a pixel is masked out if the soil surface is bare but frozen, which inhibits $F(A_f)$ or in the presence of any snow coverage (A_s). Unlike existing F models, vegetation indices and fixed vegetation coefficients in the erodibility parameter E are unnecessary and not used (Text S3 in Supporting Information S1; Chappell, Webb, Hennen, Zender, et al., 2023). Furthermore, we do not apply preferential dust source masks to pre-condition the magnitude and geographical distribution of F. The classical dust emission modeling (F_{TEM}) used here is described in standard workflows (Darmenova et al., 2009) and included in Text S3 in Supporting Information S1.

In the absence of information to parameterize $u_{*_{ts}}$ heterogeneity at the sub-grid scale, it has long been assumed fixed over space within surface texture type, and considered static over time. The ground is assumed to supply

19448007, 2024, 5, Downloaded from https://agupubs.onlinelibrary.wiley.com/doi/10.1029/2023GL106540 by Freie Universitaet Berlin, Wiley Online Library on [12/04/2024]. See the Terms and Conditions (https://onlinelibrary.wiley.com/terms-and-conditions) on Wiley Online Library for rules of use; OA articles are governed by the applicable Creative Commons License

sediment, which is loose, dry and available infinitely. These assumptions are unrealistic in dust source regions (Chappell et al., 2007; Chappell et al., 2005, 2006; Gillette et al., 2001; Sekiyama et al., 2023; Vos et al., 2020; Webb and Strong, 2011). In the absence of improved and areal $u_{*_{ts}}$, we follow recent F developments (Chappell, Webb, Hennen, Schepanski, et al., 2023; Chappell, Webb, Hennen, Zender, et al., 2023; Hennen et al., 2022; Hennen et al., 2023) and fit a logarithmic function to F_{AEM} and correct for over-estimation in F_{cal} (Chappell, Webb, Hennen, Schepanski, et al., 2023) due to assumptions about model scale, entrainment and sediment supply

$$Log_{10}\,(F_{cal}) = 1.13 Log_{10}\,(F_{AEM}) - 3.05. \quad (4)$$

The F_{cal} is calibrated against dust emission point source (DPS) data retrieved from satellite observations (Chappell, Webb, Hennen, Schepanski, et al., 2023) providing a reasonable (RMSE = ±3.80 kg m^{-2} y^{-1}) basis for global estimation of F_{cal} (Chappell, Webb, Hennen, Schepanski, et al., 2023).

2.4. Data for Implementing Dust Emission Modeling

The albedo-based approach provides areal estimated u_{s*}/U_h every day, every 0.5 km, across Earth's land surface. Albedo (MCD43A1 Collection 6) is available from MODIS aboard polar-orbiting satellites which cause incomplete coverage. However, the variation in albedo-based roughness at the daily-weekly scale is sufficiently small that we were able to smooth the available data weekly, to improve the coverage. MODIS albedo is area-integrated and scales linearly (Case 1; Raupach & Lu, 2004). For a given day with 0.5 km pixels, albedo is reprojected to pixels at >0.5 km and then calibrated to provide areal estimates of u_{s*}/U_h (Equation S1 in Supporting Information S1) for F_{cal}. The reprojection forces each albedo image with a given pixel resolution (e.g., 0.5 km) to be computed to a different (e.g., 5 km) pixel resolution which is equivalent to resampling using a bilinear interpolation. We repeat this process for all albedo images, for all resolutions in our study (0.5 km, 5 km, 11 km, 28 km, 55 km, 111 km, and 278 km) to examine F resolution dependency. For consistency with comparisons across these resolutions, we use a spatial restriction set to the largest 278 km resolution, applied to all smaller resolutions.

We implemented F_{cal} and F_{TEM} with areal mean wind fields (at 10 m height), soil moisture (0–7 cm depth) and soil surface temperature from the latest ERA5-Land data (Muñoz-Sabater et al., 2021) (resolution: hourly; 0.1°). For consistency with the daily MODIS albedo data, we converted ERA5-Land hourly to daily data and used wind maxima to better approximate the gusts which cause sediment transport and dust emission. The coverage of snow ranges between 0 and 1 and we applied the MODIS Normalized Difference Snow Index (Hall et al., 2016) (MOD10A1 Terra, daily at 500 m). We used soil surface temperature with a threshold of 273.15 K above which fluxes may occur. Soil clay content (250 m pixels) was represented with a digital soil texture map (Dai et al., 2019; Hengl et al., 2017). Consistent with the treatment of the albedo data, we reprojected these driving variables in the same way. Notably, for grid resolutions which were finer than the native grid resolutions (0.5 and 5 km) of the driving variables, we did not use any downscaling. We recognize that these driving variables are unlikely to scale linearly and therefore will not provide the most accurate values at different resolutions. Nevertheless, these reprojected driving variables were applied consistently to both F_{cal} and F_{TEM}. This approach enabled us to demonstrate the performance of scaling u_{s*} and its relative impact on dust emission across different resolutions.

3. Results and Discussion

3.1. Global Seasonal Differences in Dust Emission With Resolution

The pattern and magnitude in the daily values, aggregated to mean monthly u_{s*} normalized by wind speed (u_{s*}/U_h) during 2022, is similar for each resolution up to 111 km (Figure 1a). The similar pattern indicates that on average aerodynamic roughness is largest (u_{s*}/U_h is smallest) during March–May than in any other season. In contrast, u_{s*}/U_h (for equivalence) in the classical approach is "tuned" to a large value by assuming a smooth land surface devoid of vegetation fixed over space and static over time (z_0 = 100 μm and z_{0s} = 33.3 μm) which fixes $R(z_0) \approx 0.91$ and therefore fixes u_{s*}/U_h (Figure 1b).

The linear upscaling of albedo calibrated to u_{s*}/U_h is evidently largely independent of resolution up to 111 km. Consequently, the Q_{AEM} (Equation 2) is also largest during boreal spring (Figure 1c). More importantly, up to and including 55 km resolution, the Q_{AEM} displays little resolution dependence all year. At 111 km and 278 km resolution, resolution dependency occurs in all months and the magnitude of that dependency is proportional to the magnitude of Q_{AEM} (Figure 1c). These differences are also evident in the u_{s*}/U_h indicating that at resolutions

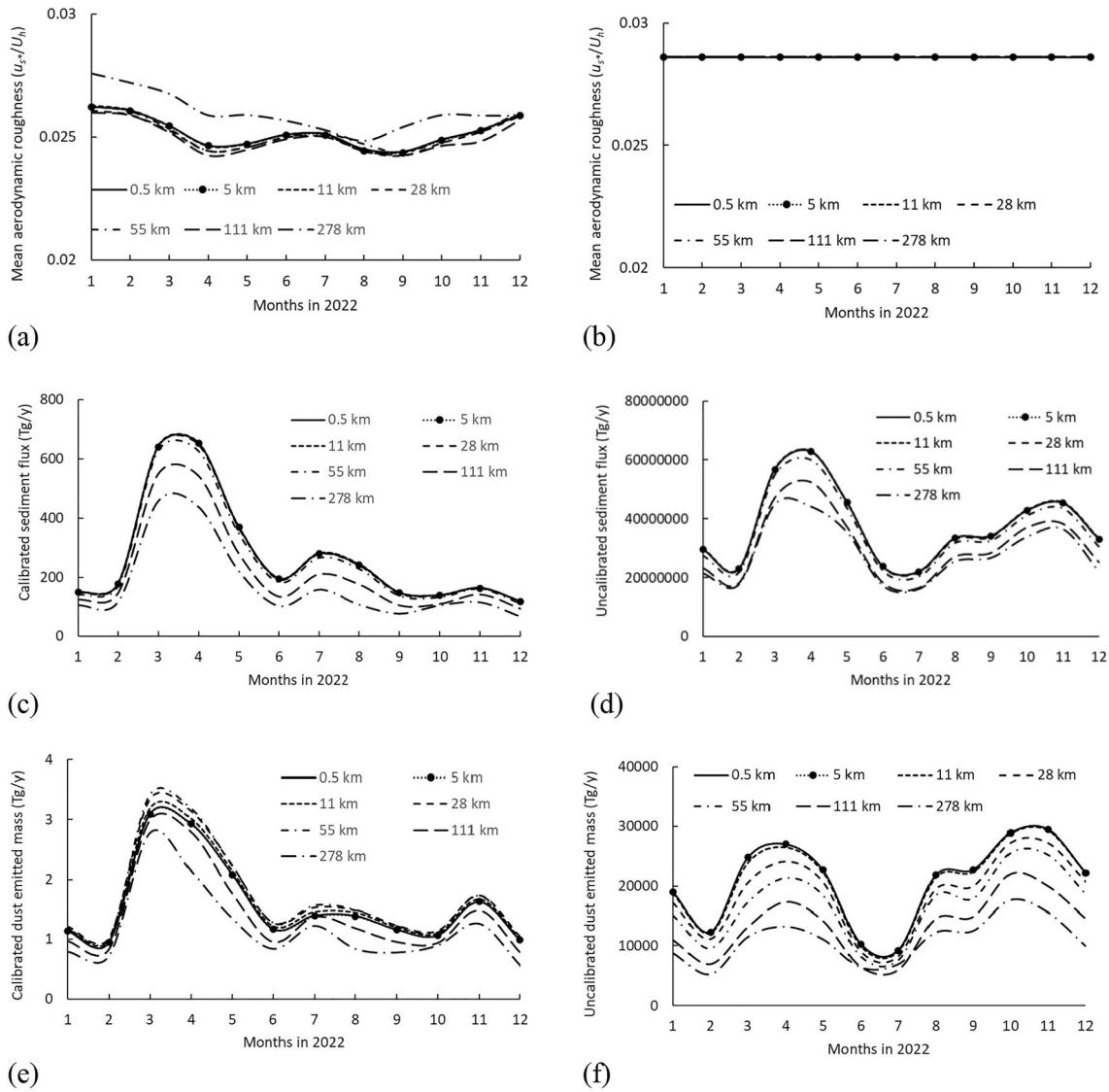

Figure 1. Seasonality of monthly 2022 dust emission for different resolutions (0.5 km, 5 km, 11 km, 28 km, 55 km, 111 km, and 278 km) using albedo-based F_{cal} modeling (left column) and uncalibrated F_{TEM} (right column) using upscaled soil surface wind friction velocity normalized by wind speed (u_{s*}/U_h; (a) and (b), sediment flux Q; (c) and (d) and dust emission (F; e and f).

of 111 km and above, the information content in the roughness has changed. This is very likely caused by differences in the sources of landscape variability for example, fundamental differences in ecoregion scales. In contrast, seasonality in Q_{TEM} is caused entirely by wind speed, not attenuated by roughness, and explains the omission of the July mode and the erroneous dominance of the November mode (Figure 1d). The difference between Q_{AEM} and Q_{TEM} demonstrates the influence of aerodynamic roughness included and omitted, respectively (Figures 1c and 1d).

There is little resolution dependence in total F_{cal} < 111 km resolution (Figure 1e), without any modifications to the wind fields. The linear scaling of albedo calibrated to u_{s*}/U_h has overcome the non-linear scaling of F in all but the largest resolutions. In contrast, F_{TEM} has a much larger response to different resolutions caused by the non-linearity in upscaling parameters (Figure 1f; cf. Chappell, Webb, Hennen, Zender, et al., 2023). Of greater concern for modeling precision is that the seasonality of F_{TEM} is bimodal (dominated by wind) in contrast to F_{cal} (interacting wind and roughness).

19448007, 2024, 5, Downloaded from https://agupubs.onlinelibrary.wiley.com/doi/10.1029/2023GL106540 by Freie Universitaet Berlin, Wiley Online Library on [12/04/2024]. See the Terms and Conditions (https://onlinelibrary.wiley.com/terms-and-conditions) on Wiley Online Library for rules of use; OA articles are governed by the applicable Creative Commons License

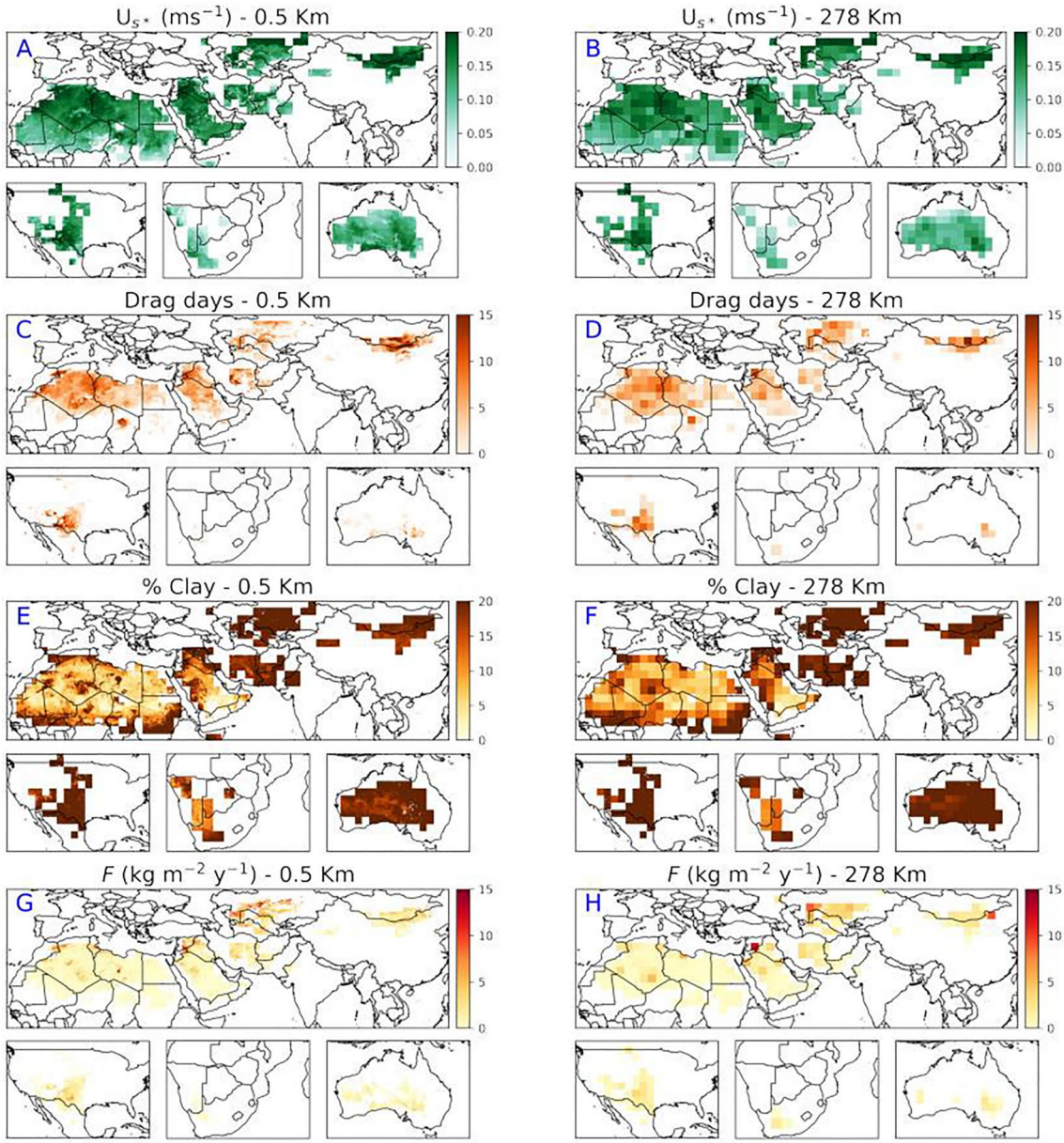

Figure 2. For March 2022, using 0.5 km (left column) and 278 km (right column) model resolution and spatially restricting to the latter, the soil surface wind friction velocity (u_{s*} m s^{-1}; a and b), the number of "drag days" when soil surface wind friction velocity exceeds the sediment entrainment threshold ($u_{s*}>u_{*ts}(d)H(w)$ fixing d = 125 μm; c and d), soil clay content restricted to a 20% maximum (e) and (f) and calibrated albedo-based dust emission (F_{cal} kg m^{-2} y^{-1}; g and h). The driving variables are reprojected by forcing the images at 0.5 km to be computed at 278 km.

The seasonality of albedo-based F_{cal} < 111 km resolution shows little resolution dependence during June–August months and to a lesser extent also during December–February. In contrast, F_{cal} > 111 km is more resolution dependent during March–April and to a lesser extent during October–November. Since resolution dependency is much less evident in u_{s*} than in Q_{AEM}, the resolution dependency is isolated (Equation 2) to grain-scale $u_{*_{ts}}H$. As resolution increases the influence of $u_{*_{ts}}H$ increases (Equation 2) becoming increasingly resolution dependent. Furthermore, the sequence of Q_{AEM} by resolution (Figure 1c) is different to that of F_{cal} (Figure 1e) indicating that the controlling factor responsible for resolution dependency of F_{cal} is different from Q_{AEM}. The Q_{AEM} is converted to F_{AEM} using a grain-scale empirical sandblasting efficiency (Equation 3) as a proportion of soil clay content. Although provided over area (250 m pixels), relative to the large resolutions considered here, this is point support. The sandblasting efficiency increases by nearly 3 orders of magnitude as soil clay content increases from 0% to

19448007, 2024, 5, Downloaded from https://agupubs.onlinelibrary.wiley.com/doi/10.1029/2023GL106540 by Freie Universitaet Berlin, Wiley Online Library on [12/04/2024]. See the Terms and Conditions (https://onlinelibrary.wiley.com/terms-and-conditions) on Wiley Online Library for rules of use; OA articles are governed by the applicable Creative Commons License

19448007, 2024, 5, Downloaded from https://agupubs.onlinelibrary.wiley.com/doi/10.1029/2023GL106540 by Freie Universitaet Berlin, Wiley Online Library on [12/04/2024]. See the Terms and Conditions (https://onlinelibrary.wiley.com/terms-and-conditions) on Wiley Online Library for rules of use; OA articles are governed by the applicable Creative Commons License

Table 1
Calibrated Total Emitted Mass (Tg y^{-1}) During 2022 for Model Resolutions (0.5 km, 5 km, 11 km, 28 km, 55 km, 111 km, and 278 km) of the Main Global Dust Source Regions Using Upscaled Albedo Calibrated to Wind Friction Velocity

Dust emission (Tg y^{-1})	0.5 km (A)	5 km (B)	11 km (C)	28 km (D)	55 km (E)	111 km (F)	278 km (G)	Diff. (A–G)	%
Australia	4.33	4.33	4.42	4.49	4.42	3.27	2.38	−1.95	+40.16
Central Asia	1.24	1.24	1.24	1.25	1.25	1.09	1.01	−0.23	+4.66
East Asia	2.44	2.45	2.50	2.70	2.68	2.38	1.52	−0.91	+18.77
Europe	0.00	0.00	0.00	0.00	0.00	0.00	0.00	0.00	0.00
India	0.04	0.04	0.04	0.04	0.04	0.04	0.03	−0.01	+0.13
Middle East	3.73	3.70	3.86	3.98	4.06	3.78	3.12	−0.61	+12.46
North Africa	3.23	3.22	3.40	3.56	3.77	3.07	2.85	−0.38	+7.87
North America	2.69	2.68	2.73	2.83	2.81	2.28	1.77	−0.91	+18.79
South America	1.20	1.19	1.23	1.37	1.25	0.99	1.28	+0.09	−1.79
Sthn Africa	0.10	0.10	0.11	0.12	0.10	0.10	0.15	+0.05	−1.03
Total	18.99	18.95	19.54	20.33	20.38	16.99	14.13	−4.86	100.00
Difference		−0.04	+0.55	+1.35	+1.39	−2.00	−4.86		
%		−0.20	+2.89	+7.10	+7.34	−10.52	−25.60		

20% (Zender et al., 2003). Therefore, the increase in F_{cal} at finer resolutions (0.5 and 5 km; inconsistent with Q_{AEM}), is a consequence of the additional incompatibility between the grain-scale, clay-driven sandblasting and its areal implementation. It is also very likely that the sequence differences in F_{cal} and Q_{AEM} between resolution, is caused by using native 11 km winds with the finer (0.5 and 5 km) albedo-based roughness. We investigate the spatial distribution of these resolution dependent processes next. Given the word limit, we include a summary of results from the classical approach in the supplement and only briefly refer to them below.

3.2. Regional Spatial Differences in Dust Emission With Resolution

We mapped the factors controlling F_{cal} at two resolutions (Figure 2) displayed spatially restricted to 278 km resolution. We consider the dominant March dust mode (from Figure 1) to make differences between models clear without aggregations across other months. The March maximum u_{s*} in North Africa is smaller than those in Central and East Asia. The 0.5 km resolution is very similar to that at 278 km across all the major dust producing regions (Figures 2a and 2b). The number of "drag days", when soil surface wind friction velocity exceeds the sediment entrainment threshold ($u_{s*}>u_{*ts}(d)H(w)$ assuming for simplicity values between d = 50–125 μm are similar, we used d = 125 μm), are also quite similar between these resolutions and across regions (Figures 2c and 2d). However, notable differences in "drag days" between resolutions in Australia and particularly the Middle East and North Africa have evidently caused the resolution dependency we noted earlier in the global seasonality of Q_{AEM} (Figure 1c). The clay content is much smaller in North Africa than other global dust source regions (Chappell, Webb, Hennen, Schepanski, et al., 2023). The clay content is similar between resolutions, indicating that the combination of the Q_{AEM} differences and the clay differences influence the F_{cal} differences with resolution (Figures 2e and 2f). The combination of small clay content and intermediate u_{s*} causes March F_{cal} to be larger in regions other than North Africa (Chappell, Webb, Hennen, Schepanski, et al., 2023). Overall, the F_{cal} maps show very similar spatial distributions regardless of resolution (Figures 2g and 2h). However, missing F_{cal} is evident in Australia and Central and East Asia and the largest magnitude difference occurs in North Africa and North America. We quantify F_{cal} by region and resolution next.

The amount of F_{cal} for the year 2022, by region and by resolution is shown in Table 1 (uncalibrated F_{TEM} are shown in Text S4 in Supporting Information S1; Table S1 in Supporting Information S1). At 0.5 km resolution, the total F_{cal} is 19 Tg y^{-1}, broadly consistent with the recent global albedo-based average (2001–2020) F_{cal} and its uncertainty (29.1 ± 14.9 Tg y^{-1}; Chappell, Webb, Hennen, Schepanski, et al., 2023; Chappell, Webb, Hennen, Zender, et al., 2023). The amount estimated here is smaller than that recent estimate because we consider only the year 2022 and because the 278 km spatial restriction excludes coastal regions (Figure 2). With resolutions ≤11 km there is little difference in total F_{cal} (0.55 Tg y^{-1}; 2.89%) which is due to the native wind speed scale of 11 km

19448007, 2024, 5, Downloaded from https://agupubs.onlinelibrary.wiley.com/doi/10.1029/2023GL106540 by Freie Universitaet Berlin, Wiley Online Library on [12/04/2024]. See the Terms and Conditions (https://onlinelibrary.wiley.com/terms-and-conditions) on Wiley Online Library for rules of use; OA articles are governed by the applicable Creative Commons License

being larger than those fine resolutions. At model resolutions >11 km the total F_{cal} doubles to the largest difference of −4.86 Tg y^{-1} (−25.6%) when comparing 0.5–278 km resolution. However, −4.86 Tg y^{-1} is similar to the F_{cal} model uncertainty (±3.8 Tg y^{-1}) and approximately one third of our recent global F_{cal} uncertainty (±14.9 Tg y^{-1}). Without modifying wind fields, global F_{cal} decreased by only 2 Tg y^{-1} (10.5%) from 0.5 to 111 km resolution. Our results represent fully dynamic F_{cal} that is, spatio-temporal variation in driving variables across all scales of soil and vegetation. Our F_{cal} results are around one third of the ∼29% decrease for the smaller range of 28–110 km resolution in F_{TEM} (Table S1 in Supporting Information S1) and those elsewhere (Feng et al., 2022). Our F_{TEM} calculations showed −96% difference between 0.5 and 278 km which demonstrates considerably more resolution dependency than the F_{cal} (Table S1 in Supporting Information S1). That resolution dependency of F_{TEM} is primarily because dust emission has a fixed drag partition, controlling the wind friction velocity, which does not change with scale. Ridley et al. (2013) showed similarly large differences in their F across a smaller range of resolutions (33% from 28–200 km). However, their experiments assumed uniform soil texture and uniform surface roughness which reduced their experiments sensitivity to land surface properties (Ridley et al., 2013). Decoupling wind speed from aerodynamic roughness (changing over space and time) in that way, will introduce additional uncertainty in the parameterization used to reconcile differences in F between resolutions.

We explained elsewhere how and why North Africa and the Middle East are not persistently the largest global sources of F, and that regional F contributions shift seasonally (Chappell, Webb, Hennen, Schepanski, et al., 2023). At 0.5 km resolution, our largest F_{cal} is from Australia followed closely by the Middle East and North Africa (Table 1). At 278 km resolution, the largest amount of global F is from the Middle East, North Africa and then Australia (Table 1). The dominance of Australia at 0.5 km is explained by our use of only a single year and interannual variability in dust emission, and because the F_{cal} are restricted spatially using the 278 km resolution which preferentially focuses on continental interiors due to pixel edge effects (Figure 2). Australian F_{cal} naturally occurs away from the highly vegetated coastal regions. Consequently, using this 278 km resolution spatial restriction gives preference to F_{cal} from continental interiors and causes Australia to have the most dust in these simulations. However, the purpose of the simulations is to compare the relative differences. Australia has the greatest difference in F_{cal} between the 0.5 and 278 km resolution of 1.95 Tg y^{-1} (40.16% of the total difference Table 1). The greatest resolution dependence is very likely caused by Australia having the largest differences in landscape variability at 278 km for example, with fundamental differences in ecoregion scales at 278 km. East Asia and North America have the next largest differences (∼0.91 Tg y^{-1} around 19%; Table 1) in F_{cal} caused by these resolutions.

4. Conclusion

Our calibrated albedo-based dust emission (F_{cal}) magnitude, spatial distribution, and seasonality does not depend upon resolution (<111 km). Area-integrated albedo scales linearly with resolution and its relation with sheltering represents sub-grid scale heterogeneity in u_{s*}. This straightforward scaling in a global F_{cal} produced remarkably consistent results across resolution, with fewer parameters than F_{TEM}, making the approach suitable for large scale dust cycle modeling and operational weather forecasting. At 111 km and particularly at 278 km resolution, linear scaling of albedo and calibration to u_{s*}/U_h behaves differently because of a fundamental difference in the landscape heterogeneity for example, ecoregion scale.

This dust emission modeling approach is largely resolution independent without adjusting wind fields, unlike previous approaches. Dust emission is not dependent solely on wind speed (U_h), but on u_{s*} which represents aerodynamic sheltering. The long-standing focus on adjusting the wind field excludes the feedback and interaction with aerodynamic roughness changes over space-time. Consequently, attempts to improve F models using new re-gridded wind field parameterizations do not adequately account for the sub-grid scale heterogeneity in the u_{s*}, which drive F. Hence, existing approaches to large scale modeling of dust emission retain considerable resolution dependence.

Overcoming non-linearity in scaling u_{s*} already demonstrated elsewhere the importance of seasonally shifting global dust source regions with many other arising implications for this largely resolution independent F modeling. ESMs cycling dust with this new resolution independent modeling will very likely reduce uncertainty and correctly represent dust types and seasonality particularly those overlooked in the southern hemisphere. These ESMs will then be able to tackle previously unresolved issues for example, Southern Ocean productivity

19448007, 2024, 5, Downloaded from https://agupubs.onlinelibrary.wiley.com/doi/10.1029/2023GL106540 by Freie Universitaet Berlin, Wiley Online Library on [12/04/2024]. See the Terms and Conditions (https://onlinelibrary.wiley.com/terms-and-conditions) on Wiley Online Library for rules of use; OA articles are governed by the applicable Creative Commons License

associated with quartz and iron hypotheses from dust sources. Similarly, properly coupling albedo-based dust cycling with energy-driven ESMs offers new opportunities for feedbacks and interactions. Furthermore, dust aerosol modeling accounting for sub-grid scale heterogeneity with this approach is expected to provide more accurate air quality forecasts than classical approaches.

Future improvements in F modeling must overcome the remaining non-linearity of grain-scale parameterizations being re-gridded over large scales. Remaining resolution dependency in Q seasonality was evident in regional differences in "drag days" and in F_{cal} by grain-scale sandblasting and is also likely to occur in the soil moisture function $H(w)$ and wind speed U_h. The long-standing $u_{*\mathrm{ts}}$ and sandblasting parameterizations are responsible for the remaining F resolution dependence important for dust cycle models. Until the $u_{*\mathrm{ts}}$ and sandblasting are parameterized non-linearly (and ideally dynamically) over area, F modeling will remain poorly constrained and resolution dependent.

Code Availability

The dust emission code is archived as a text file using Zenodo (where the code will not run without access to the Google Earth Engine) using the DOI: doi.org/10.5281/zenodo.5626825.

Data Availability Statement

The dust emission modeling was performed in the Google Earth Engine (GEE) with the following data. To mask the sea from the land we used land cover classification (MODIS/051/MCD12Q1) (Friedl, 2022). Albedo was from MODIS/006/MCD43A1 (Schaaf and Wang, 2015). Snow cover was from MODIS/006/MOD10A1 (Hall et al., 2016). Normalized Difference Vegetation Index (NDVI) data was from MODIS/MOD09GA_006_NDVI (Vermote and Wolfe, 2015). The u and v components of wind speed at 10 m, volumetric soil water and soil temperature were from ECMWF/ERA5_LAND/HOURLY (C3S, 2022). The clay content from the ISRIC Soilgrids data (Hengl et al., 2017) was uploaded privately to the Google Earth Engine.

Conflict of Interest

The authors declare no conflicts of interest relevant to this study.

Acknowledgments
We thank Google for use of the Earth Engine and thank the following organizations for use of their data: NCEP, NASA EOSDIS LP DAAC; USGS/EROS; ISRIC SoilGrids. We thank two anonymous reviewers who contributed to improving the clarity of the manuscript. Funding for the work was provided to AC by the Natural Environmental Research Council (NE/T002263/1).

References

Albani, S., Mahowald, N. M., Perry, A. T., Scanza, R. A., Zender, C. S., Heavens, N. G., et al. (2014). Improved dust representation in the Community Atmosphere Model. *Journal of Advances in Modeling Earth Systems*, *6*(3), 541–570. https://doi.org/10.1002/2013ms000279

(C3S), C. C. C. S. (2022). ERA5-Land hourly data from 1950 to present, edited by C. C. C. S. C. S. C. D. S. (CDS). https://doi.org/10.24381/cds.e2161bac

Cakmur, R. V., Miller, R. L., & Torres, O. (2004). Incorporating the effect of small-scale circulations upon dust emission in an atmospheric general circulation model. *Journal of Geophysical Research*, *109*(D7). https://doi.org/10.1029/2003JD004067

Chappell, A., Strong, C., McTainsh, G., & Leys, J. (2007). Detecting induced in situ erodibility of a dust-producing playa in Australia using a bi-directional soil spectral reflectance model. *Remote Sensing of Environment*, *106*(4), 508–524. https://doi.org/10.1016/j.rse.2006.09.009

Chappell, A., & Webb, N. P. (2016). Using albedo to reform wind erosion modelling, mapping and monitoring. *Aeolian Research*, *23*, 63–78. https://doi.org/10.1016/j.aeolia.2016.09.006

Chappell, A., Webb, N. P., Hennen, M., Schepanski, K., Ciais, P., Balkanski, Y., et al. (2023). Satellites reveal Earth's seasonally shifting dust emission sources. *The Science of the Total Environment*, *883*, 163452. https://doi.org/10.1016/j.scitotenv.2023.163452

Chappell, A., Webb, N. P., Hennen, M., Zender, C. S., Ciais, P., Schepanski, K., et al. (2023). Elucidating hidden and enduring weaknesses in dust emission modeling. *Journal of Geophysical Research: Atmospheres*, *128*(17), e2023JD038584. https://doi.org/10.1029/2023JD038584

Chappell, A., Webb, N. P., Leys, J. F., Waters, C. M., Orgill, S., & Eyres, M. J. (2019). Minimising soil organic carbon erosion by wind is critical for land degradation neutrality. *Environmental Science and Policy*, *93*, 43–52. https://doi.org/10.1016/j.envsci.2018.12.020

Chappell, A., Zobeck, T. M., & Brunner, G. (2005). Using on-nadir spectral reflectance to detect soil surface changes induced by simulated rainfall and wind tunnel abrasion. *Earth Surface Processes and Landforms*, *30*(4), 489–511. https://doi.org/10.1002/esp.1185

Chappell, A., Zobeck, T. M., & Brunner, G. (2006). Using bi-directional soil spectral reflectance to model soil surface changes induced by rainfall and wind-tunnel abrasion. *Remote Sensing of Environment*, *102*(3), 328–343. https://doi.org/10.1016/j.rse.2006.02.020

Cowie, S. M., Marsham, J. H., & Knippertz, P. (2015). The importance of rare, high-wind events for dust uplift in northern Africa. *Geophysical Research Letters*, *42*(19), 8208–8215. https://doi.org/10.1002/2015GL065819

Dai, Y., Shangguan, W., Wei, N., Xin, Q., Yuan, H., Zhang, S., et al. (2019). A review of the global soil property maps for Earth system models. *SOIL*, *5*(2), 137–158. https://doi.org/10.5194/soil-5-137-2019

Darmenova, K., Sokolik, I. N., Shao, Y., Marticorena, B., & Bergametti, G. (2009). Development of a physically based dust emission module within the Weather Research and Forecasting (WRF) model: Assessment of dust emission parameterizations and input parameters for source regions in Central and East Asia. *Journal of Geophysical Research*, *114*(D14). https://doi.org/10.1029/2008jd011236

de Vrese, P., & Hagemann, S. (2016). Explicit representation of spatial subgrid-scale heterogeneity in an ESM. *Journal of Hydrometeorology*, *17*(5), 1357–1371. https://doi.org/10.1175/jhm-d-15-0080.1

Fécan, F., Marticorena, B., & Bergametti, G. (1999). Parametrization of the increase of the aeolian erosion threshold wind friction velocity due to soil moisture for arid and semi-arid areas. *Annals of Geophysics*, *17*(1), 149–157. https://doi.org/10.1007/s00585-999-0149-7

Feng, Y., Wang, H., Rasch, P. J., Zhang, K., Lin, W., Tang, Q., et al. (2022). Global dust cycle and direct radiative effect in E3SM version 1: Impact of increasing model resolution. *Journal of Advances in Modeling Earth Systems*, *14*(7), e2021MS002909. https://doi.org/10.1029/2021MS002909

Friedl, M., & Sulla-Menashe, D. (2022). MODIS/Terra+Aqua Land Cover Type Yearly L3 Global 500 m SIN Grid V061. [Dataset]. edited by N. E. L. P. DAAC. https://doi.org/10.5067/MODIS/MCD12Q1.061

Gillette, D. A., Niemeyer, T. C., & Helm, P. J. (2001). Supply-limited horizontal sand drift at an ephemerally crusted, unvegetated saline playa. *Journal of Geophysical Research*, *106*(D16), 18085–18098. https://doi.org/10.1029/2000JD900324

Gotway, C. A., & Young, L. J. (2002). Combining incompatible spatial data. *Journal of the American Statistical Association*, *97*(458), 632–648. https://doi.org/10.1198/016214502760047140

Grini, A., Myhre, G., Zender, C. S., & Isaksen, I. S. A. (2005). Model simulations of dust sources and transport in the global atmosphere: Effects of soil erodibility and wind speed variability. *Journal of Geophysical Research*, *110*(D2). https://doi.org/10.1029/2004JD005037

Hall, D. K., Salomonson, V. V., & Riggs, G. A. (2016). *MODIS/Terra snow cover daily L3 global 500m grid. Version 6*. NASA National Snow and Ice Data Center Distributed Active Archive Center.

Hengl, T., Mendes de Jesus, J., Heuvelink, G. B. M., Ruiperez Gonzalez, M., Kilibarda, M., Blagotić, A., et al. (2017). SoilGrids250m: Global gridded soil information based on machine learning. *PLoS One*, *12*(2), e0169748. https://doi.org/10.1371/journal.pone.0169748

Hennen, M., Chappell, A., Edwards, B. L., Faist, A. M., Kandakji, T., Baddock, M. C., et al. (2022). A North American dust emission climatology (2001–2020) calibrated to dust point sources from satellite observations. *Aeolian Research*, *54*, 100766. https://doi.org/10.1016/j.aeolia.2021.100766

Hennen, M., Chappell, A., & Webb, N. P. (2023). Modelled direct causes of dust emission change (2001–2020) in southwestern USA and implications for management. *Aeolian Research*, *60*, 100852. https://doi.org/10.1016/j.aeolia.2022.100852

Huneeus, N., Schulz, M., Balkanski, Y., Griesfeller, J., Prospero, J., Kinne, S., et al. (2011). Global dust model intercomparison in AeroCom phase I. *Atmospheric Chemistry and Physics*, *11*(15), 7781–7816. https://doi.org/10.5194/acp-11-7781-2011

Joussaume, S. (1990). Three-dimensional simulations of the atmospheric cycle of desert dust particles using a general circulation model. *Journal of Geophysical Research*, *95*(D2), 1909–1941. https://doi.org/10.1029/JD095iD02p01909

Kyriakidis, P. C., & Yoo, E.-H. (2005). Geostatistical prediction and simulation of point values from areal data. *Geographical Analysis*, *37*(2), 124–151. https://doi.org/10.1111/j.1538-4632.2005.00633.x

LeGrand, S. L., Letcher, T. W., Okin, G. S., Webb, N. P., Gallagher, A. R., Dhital, S., et al. (2023). Application of a satellite-retrieved sheltering parameterization (v1.0) for dust event simulation with WRF-Chem v4.1. *Geoscientific Model Development*, *16*(3), 1009–1038. https://doi.org/10.5194/gmd-16-1009-2023

Leung, D. M., Kok, J. F., Longlei, L., Okin, G. S., Prigent, C., Klose, M., et al. (2023). A new process-based and scale-aware desert dust emission scheme for global climate models – Part I: Description and evaluation against inverse modeling emissions. *Atmospheric Chemistry and Physics*, *23*(11), 6487–6523. https://doi.org/10.5194/acp-23-6487-2023

Li, J., Kandakji, T., Lee, J. A., Tatarko, J., Blackwell, J., Gill, T. E., & Collins, J. D. (2018). Blowing dust and highway safety in the southwestern United States: Characteristics of dust emission "hotspots" and management implications. *The Science of the Total Environment*, *621*, 1023–1032. https://doi.org/10.1016/j.scitotenv.2017.10.124

Mahowald, N. M., Kloster, S., Engelstaedter, S., Moore, J. K., Mukhopadhyay, S., McConnell, J. R., et al. (2010). Observed 20th century desert dust variability: Impact on climate and biogeochemistry. *Atmospheric Chemistry and Physics*, *10*(22), 10875–10893. https://doi.org/10.5194/acp-10-10875-2010

Marticorena, B., & Bergametti, G. (1995). Modeling the atmospheric dust cycle: 1. Design of a soil-derived dust emission scheme. *Journal of Geophysical Research: Atmospheres*, *100*(D8), 16415–16430. https://doi.org/10.1029/95jd00690

Meng, J., Martin, R. V., Ginoux, P., Hammer, M., Sulprizio, M. P., Ridley, D. A., & van Donkelaar, A. (2021). Grid-independent high-resolution dust emissions (v1.0) for chemical transport models: Application to GEOS-Chem (12.5.0). *Geoscientific Model Development*, *14*(7), 4249–4260. https://doi.org/10.5194/gmd-14-4249-2021

Menut, L. (2018). Modeling of mineral dust emissions with a Weibull wind speed distribution including subgrid-scale orography variance. *Journal of Atmospheric and Oceanic Technology*, *35*(6), 1221–1236. https://doi.org/10.1175/JTECH-D-17-0173.1

Muñoz-Sabater, J., Dutra, E., Agustí-Panareda, A., Albergel, C., Arduini, G., Balsamo, G., et al. (2021). ERA5-Land: A state-of-the-art global reanalysis dataset for land applications. *Earth System Science Data*, *13*(9), 4349–4383. https://doi.org/10.5194/essd-13-4349-2021

Namikas, S., & Sherman, D. J. (1997). Predicting aeolian sand transport: Revisiting the white model. *Earth Surface Processes and Landforms*, *22*(6), 601–604. https://doi.org/10.1002/(sici)1096-9837(199706)22:6<601::Aid-esp783>3.0.Co;2-5

Pi, H., Webb, N. P., Huggins, D. R., & Sharratt, B. (2020). Critical standing crop residue amounts for wind erosion control in the inland Pacific Northwest, USA. *Catena*, *195*, 104742. https://doi.org/10.1016/j.catena.2020.104742

Raupach, M., & Finnigan, J. (1995). Scale issues in boundary-layer meteorology: Surface energy balances in heterogeneous terrain. *Hydrological Processes*, *9*(5–6), 589–612. https://doi.org/10.1002/hyp.3360090509

Raupach, M. R., & Lu, H. (2004). Representation of land-surface processes in aeolian transport models. *Environmental Modelling and Software*, *19*(2), 93–112. https://doi.org/10.1016/S1364-8152(03)00113-0

Ridley, D. A., Heald, C. L., Pierce, J. R., & Evans, M. J. (2013). Toward resolution-independent dust emissions in global models: Impacts on the seasonal and spatial distribution of dust. *Geophysical Research Letters*, *40*(11), 2873–2877. https://doi.org/10.1002/grl.50409

Schaaf, C., & Wang, Z. (2015). MCD43A3 MODIS/Terra+Aqua BRDF/Albedo Daily L3 Global - 500 m V006. [Dataset]. NASA EOSDIS Land Processes DAAC. https://doi.org/10.5067/MODIS/MCD43A3.006

Sekiyama, T. T., Kurosaki, Y., Kajino, M., Ishizuka, M., Buyantogtokh, B., Wu, J., & Maki, T. (2023). Improvement in dust storm simulation by considering stone coverage effects for stony deserts in East Asia. *Journal of Geophysical Research: Atmospheres*, *128*(2), e2022JD037295. https://doi.org/10.1029/2022JD037295

Shao, Y., Klose, M., & Wyrwoll, K.-H. (2013). Recent global dust trend and connections to climate forcing. *Journal of Geophysical Research: Atmospheres*, *118*(19), 11107–11118. https://doi.org/10.1002/jgrd.50836

Shao, Y., Raupach, M., & Leys, J. (1996). A model for predicting aeolian sand drift and dust entrainment on scales from paddock to region. *Soil Research*, *34*(3), 309–342. https://doi.org/10.1071/SR9960309

Shao, Y., Wyrwoll, K.-H., Chappell, A., Huang, J., Lin, Z., McTainsh, G. H., et al. (2011). Dust cycle: An emerging core theme in Earth system science. *Aeolian Research*, *2*(4), 181–204. https://doi.org/10.1016/j.aeolia.2011.02.001

19448007, 2024, 5, Downloaded from https://agupubs.onlinelibrary.wiley.com/doi/10.1029/2023GL106540 by Freie Universitaet Berlin, Wiley Online Library on [12/04/2024]. See the Terms and Conditions (https://onlinelibrary.wiley.com/terms-and-conditions) on Wiley Online Library for rules of use; OA articles are governed by the applicable Creative Commons License

Tai, A. P. K., Ma, P. H. L., Chan, Y.-C., Chow, M.-K., Ridley, D. A., & Kok, J. F. (2021). Impacts of climate and land cover variability and trends on springtime East Asian dust emission over 1982–2010: A modeling study. *Atmospheric Environment*, *254*, 118348. https://doi.org/10.1016/j.atmosenv.2021.118348

Tegen, I., & Schepanski, K. (2018). Climate feedback on aerosol emission and atmospheric concentrations. *Current Climate Change Reports*, *4*(1), 1–10. https://doi.org/10.1007/s40641-018-0086-1

Van Looy, K., Bouma, J., Herbst, M., Koestel, J., Minasny, B., Mishra, U., et al. (2017). Pedotransfer functions in Earth system science: Challenges and perspectives. *Reviews of Geophysics*, *55*(4), 1199–1256. https://doi.org/10.1002/2017RG000581

Vermote, E., & Wolfe, R. (2015). MOD09GA MODIS/Terra Surface Reflectance Daily L2G Global 1kmand 500m SIN Grid V006. [Dataset]. edited by N. E. L. P. DAAC. https://doi.org/10.5067/MODIS/MOD09GA.006

Vos, H. C., Fister, W., Eckardt, F. D., Palmer, A. R., & Kuhn, N. J. (2020). Physical crust formation on Sandy soils and their potential to reduce dust emissions from croplands. *Land*, *9*(12), 503. https://doi.org/10.3390/land9120503

Webb, N. P., Chappell, A., LeGrand, S. L., Ziegler, N. P., & Edwards, B. L. (2020). A note on the use of drag partition in aeolian transport models. *Aeolian Research*, *42*, 100560. https://doi.org/10.1016/j.aeolia.2019.100560

Webb, N. P., & Strong, C. L. (2011). Soil erodibility dynamics and its representation for wind erosion and dust emission models. *Aeolian Research*, *3*(2), 165–179. https://doi.org/10.1016/j.aeolia.2011.03.002

Wilcox, E. M., Lau, K. M., & Kim, K.-M. (2010). A northward shift of the North Atlantic Ocean Intertropical Convergence Zone in response to summertime Saharan dust outbreaks. *Geophysical Research Letters*, *37*(4). https://doi.org/10.1029/2009GL041774

Zender, C. S., Bian, H., & Newman, D. (2003). Mineral Dust Entrainment and Deposition (DEAD) model: Description and 1990s dust climatology. *Journal of Geophysical Research: Atmospheres*, *108*(D14). https://doi.org/10.1029/2002jd002775

Zhang, K., Zhao, C., Wan, H., Qian, Y., Easter, R. C., Ghan, S. J., et al. (2016). Quantifying the impact of sub-grid surface wind variability on sea salt and dust emissions in CAM5. *Geoscientific Model Development*, *9*(2), 607–632. https://doi.org/10.5194/gmd-9-607-2016

Zhou, Z., Zhang, C., Chappell, A., Zou, X., Zhang, Z., Zuo, X., et al. (2024). Using field measurements across land cover types to evaluate albedo-based wind friction velocity and estimate sediment transport. *Journal of Geophysical Research: Atmospheres*, *129*(4), e2023JD040313. https://doi.org/10.1029/2023JD040313

Ziegler, N. P., Webb, N. P., Chappell, A., & LeGrand, S. L. (2020). Scale invariance of albedo-based wind friction velocity. *Journal of Geophysical Research: Atmospheres*, *125*(16), e2019JD031978. https://doi.org/10.1029/2019jd031978

Erratum

The originally published version of this article contained a typographical error in one of the references. In all instance of the text citations and the reference for "Chappell, Webb, Hennen, Schepanski, et al., 2023," the author name "Web" should be "Webb." The errors have been corrected, and this may be considered the authoritative version of record.

19448007, 2024, 5, Downloaded from https://agupubs.onlinelibrary.wiley.com/doi/10.1029/2023GL106540 by Freie Universitaet Berlin, Wiley Online Library on [12/04/2024]. See the Terms and Conditions (https://onlinelibrary.wiley.com/terms-and-conditions) on Wiley Online Library for rules of use; OA articles are governed by the applicable Creative Commons License